

Reaction Pathway and Free Energy Profile for Cocaine Hydrolase-Catalyzed Hydrolysis of (−)-Cocaine

Junjun Liu^{†,‡} and Chang-Guo Zhan^{*,‡}

[†]Tongji School of Pharmacy, Huazhong University of Science and Technology, 13 Hangkong Road, Wuhan, Hubei 430030, P. R. China

[‡]Department of Pharmaceutical Sciences, College of Pharmacy, University of Kentucky, 789 South Limestone Street, Lexington, Kentucky 40536, United States

ABSTRACT: The reaction pathway of (−)-cocaine hydrolysis catalyzed by our recently discovered, most efficient cocaine hydrolase, which is the A199S/F227A/S287G/A328W/Y332G mutant of human butyrylcholinesterase (BChE), and the corresponding free energy profile have been studied by performing first-principles pseudobond quantum mechanical/molecular mechanical (QM/MM)-free energy (FE) calculations. On the basis of the QM/MM-FE results, the catalytic hydrolysis process consists of four major reaction steps, including the nucleophilic attack on the carbonyl carbon of the (−)-cocaine benzoyl ester by the hydroxyl group of S198, dissociation of the (−)-cocaine benzoyl ester, nucleophilic attack on the carbonyl carbon of the (−)-cocaine benzoyl ester by water, and finally the dissociation between the (−)-cocaine benzoyl group and S198 of the enzyme. The second reaction step is rate-determining. The calculated free energy barrier associated with the transition state for the rate-determining step is ~15.0 kcal/mol, which is in excellent agreement with the experimentally derived activation free energy of ~14.7 kcal/mol. The mechanistic insights obtained from the present study will be valuable for the rational design of more active cocaine hydrolase against (−)-cocaine. In particular, future efforts aiming at further increasing the catalytic activity of the enzyme against (−)-cocaine should focus on stabilization of the transition state for the second reaction step in which the benzoyl ester of (−)-cocaine dissociates.

INTRODUCTION

Cocaine is recognized as the most reinforcing drug of abuse.^{1–3} It directly affects the brain and produces a number of toxic effects at high doses. Despite intensive efforts toward education, cocaine abuse continues to be a serious public health problem.⁴ Recent surveys in the United States show that cocaine was the first on the list of causes of illicit-drug-related emergency department visits.⁵ This widely abused drug produces potent stimulation in both the central nervous system (CNS) and the cardiovascular system. The potent stimulation is followed by depression.⁶ The common effects of overdosed cocaine include respiratory depression, cardiac arrhythmia, and acute hypertension. The disastrous medical and social consequences of cocaine addiction have made the development of an anticocaine medication a high priority.^{7,8} Unfortunately, there is no FDA-approved medication specific for cocaine overdose or addiction, and the search for an effective and safe treatment continues.^{9–13}

There are two enantiomers of cocaine. One is the naturally occurring (−)-cocaine, which is biologically active. The other is the unnatural (+)-cocaine, which is biologically inactive. The classic CNS-receptor antagonist approach has failed to yield an anticocaine therapeutic agent against (−)-cocaine, due to the difficulties inherent in blocking a blocker. Nevertheless, we have developed a proof of principle for a peripheral blocker to accelerate (−)-cocaine metabolism in circulation.^{5,7,12–18} Butyrylcholinesterase (BChE) is the principal enzyme catalyzing the hydrolysis of (−)-cocaine into its biologically inactive metabolites in human plasma,¹⁶ and thus, the BChE-catalyzed hydrolysis of (−)-cocaine is the cocaine-metabolizing pathway

most suitable for amplification in the development of an anticocaine medication. However, the catalytic efficiency of wild-type BChE against (−)-cocaine is rather low ($k_{\text{cat}} = 4.1 \pm 0.4 \text{ min}^{-1}$, $K_M = 4.5 \pm 0.3 \mu\text{M}$).¹⁹

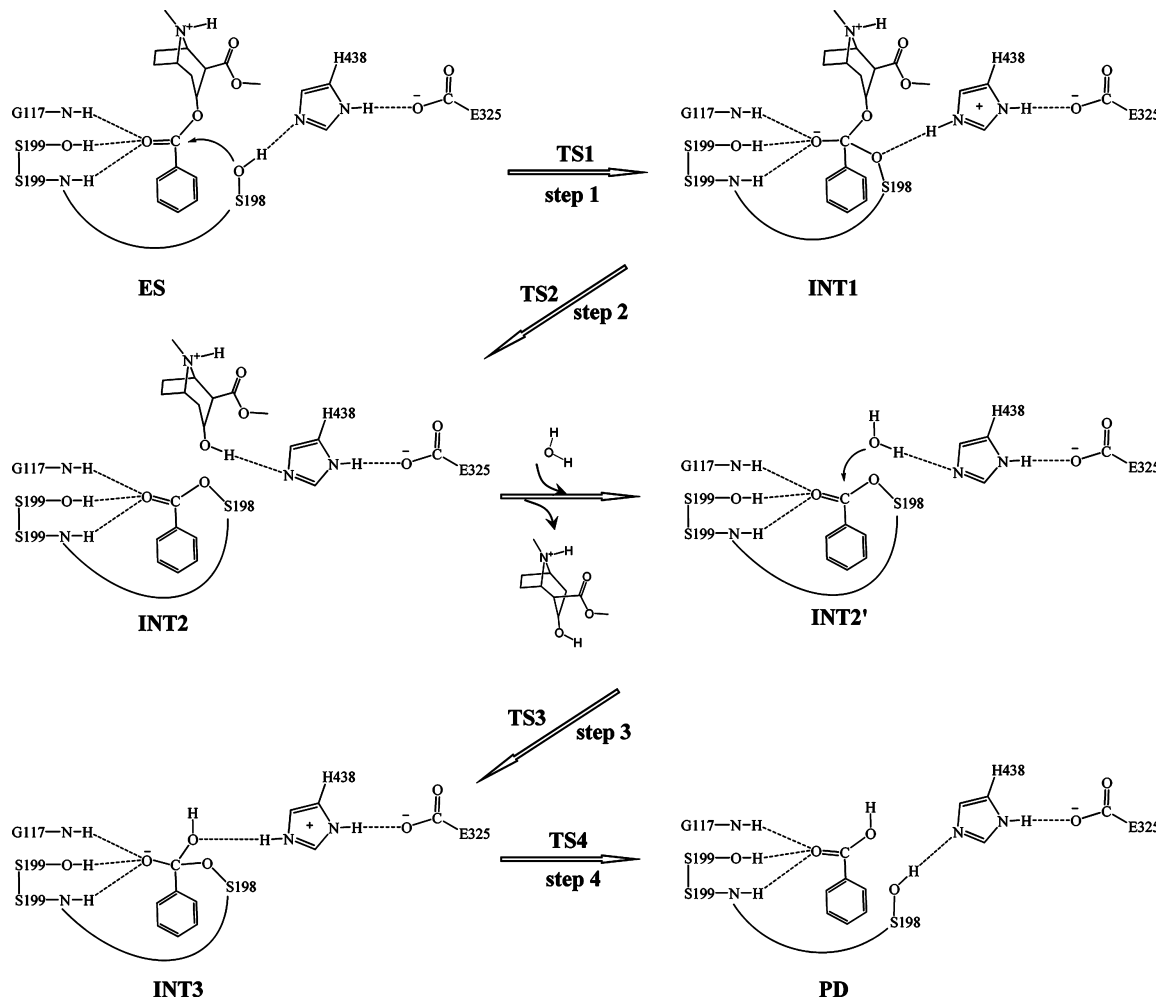
To understand the fundamental reaction mechanism for the BChE-catalyzed hydrolysis of (−)-cocaine, we have carried out extensive computational studies on wild-type BChE interacting with (−)-cocaine^{4,16,20–22} in comparison with available experimental kinetic data. Experimental kinetic analysis²³ revealed that the rate-determining step for wild-type BChE-catalyzed hydrolysis of (−)-cocaine is the formation of the enzyme–substrate complex, rather than any step of the chemical reaction process. As a result, the catalytic rate constant for wild-type BChE-catalyzed hydrolysis of (−)-cocaine is independent of the pH of the reaction solution. According to our computational results,^{4,16,21} (−)-cocaine first slides down the substrate-binding gorge of BChE to bind to W82 and stands vertically in the gorge between D70 and W82 (non-prereactive enzyme–substrate complex) and then rotates to a position in the catalytic site within a favorable distance for nucleophilic attack and hydrolysis by S198 (prereactive enzyme–substrate complex). On the basis of the free energy profiles determined by using the potential of mean force (PMF) approach,^{4,21,24} the highest free energy barrier for the prechemical reaction process is associated with the (−)-cocaine rotation in the BChE active site from the nonprereactive complex to the prereactive complex.²¹ There is no significant

Received: November 11, 2011

Published: March 6, 2012



Scheme 1. Proposed Catalytic Mechanism for the Hydrolysis of (−)-Cocaine Catalyzed by the A199S/F227A/S287G/A328W/Y332G Mutant of BChE



free energy barrier for the non-prereactive enzyme–substrate binding process.⁴ In light of the mechanistic insights, we have successfully designed and discovered a set of BChE mutants with significantly improved catalytic efficiency against (−)-cocaine.^{10,12,13,18,22,25–27} Within all cocaine-metabolizing enzymes reported in the literature so far, the most efficient one is the A199S/F227A/S287G/A328W/Y332G mutant of human BChE.¹³ It has been shown that this BChE mutant has a ~2000-fold improved catalytic efficiency¹³ against (−)-cocaine compared to the wild-type. Thus, this BChE mutant has been recognized as a true cocaine hydrolase.²⁸ The pretreatment with this BChE mutant (using a dose of 0.01 mg per mouse, i.v.) can fully protect mice from the acute toxicity of a lethal dose of cocaine (180 mg/kg, i.p.), good for cocaine overdose treatment.¹³ It is interesting for anticocaine medication development to further improve the catalytic activity of this enzyme against (−)-cocaine in order to minimize the dose required for practical anticocaine medication. The lower the enzyme dose required, the less expensive the practical medication is. In order to further improve the catalytic activity against (−)-cocaine, one first needs to understand the detailed reaction mechanism of (−)-cocaine hydrolysis catalyzed by cocaine hydrolase.

Recently, the first-principles quantum mechanical methods, in particular the combined quantum mechanical/molecular

mechanical (QM/MM) methods, have been widely applied in drug design and have been proven valuable in studying mechanistic aspects for a wide range of biomolecular systems related to drug design.^{29–34} However, it should be pointed out that, within all computational studies on the BChE-catalyzed hydrolysis of (−)-cocaine reported so far, only wild-type BChE has been subjected to the QM/MM reaction-coordinate calculations on the entire chemical reaction process.^{16,20} There has been no complete reaction-coordinate calculation on any BChE mutant against (−)-cocaine, although it has been known that the rate-determining step is no longer the (−)-cocaine rotation in the active site of the enzyme.^{4,21} One of the chemical reaction steps must be rate-determining for the cocaine hydrolase against (−)-cocaine. In the present study, we have carried out extensive computational studies using a first-principles pseudobond quantum mechanical/molecular mechanical-free energy (QM/MM-FE) approach,^{35–38} which has been demonstrated to be a powerful tool in simulating a variety of enzymes,^{13,39–51} to uncover the detailed mechanism for (−)-cocaine hydrolysis catalyzed by the A199S/F227A/S287G/A328W/Y332G mutant. On the basis of the detailed mechanistic insights obtained from our recent computational studies on the mechanisms for hydrolyses of (−)-cocaine and other carboxylic esters catalyzed by wild-type BChE and cocaine esterase (CocE),^{12,13,18,20,22,52–56} (−)-cocaine hydroly-

ysis in the A199S/F227A/S287G/A328W/Y332G mutant might undergo a very similar pathway as that in wild-type BChE,¹⁶ which consists of two major stages. The first stage is likely acylation, leading to covalent bond formation between (−)-cocaine and the enzyme and the departure of ecgonine methyl ester group from the benzoyl ester group of (−)-cocaine. The second stage is likely deacylation, resulting in the dissociation of the (−)-cocaine benzoyl ester from the enzyme, in which a water molecule acts as the nucleophile and the free state of enzyme is restored afterward.

Further, on the basis of our initial computational exploration of a possible reaction pathway for (−)-cocaine hydrolysis catalyzed by the A199S/F227A/S287G/A328W/Y332G mutant, in the present study, we proposed a working hypothesis for the more detailed reaction pathway of (−)-cocaine hydrolysis by this BChE mutant (Scheme 1). The computational results clearly reveal the detailed reaction pathway and the corresponding free energy profile for (−)-cocaine hydrolysis catalyzed by the A199S/F227A/S287G/A328W/Y332G mutant. On the basis of the free energy profile, the rate-determining reaction step has been identified. In addition, the roles of essential residues forming the catalytic triad and oxyanion hole are discussed below on the basis of the QM/MM-optimized geometries of key states of the system during the catalytic reaction process.

RESULTS AND DISCUSSION

Fundamental Reaction Pathway. Our QM/MM reaction coordinate calculations at the B3LYP/6-31G*:AMBER level revealed that the (−)-cocaine hydrolysis catalyzed by the cocaine hydrolase (the A199S/F227A/S287G/A328W/Y332G mutant of BChE) can be described in four major reaction steps. The first reaction step is the nucleophilic attack on the carbonyl carbon (C^ζ) of (−)-cocaine benzoyl ester by the O^γ atom in the S198 side chain. The second reaction step is the dissociation between the benzoyl ester and ecgonine methyl ester of (−)-cocaine. The third reaction step is the nucleophilic attack on the carbonyl carbon (C^ζ) of (−)-cocaine benzoyl ester by a water molecule. The final reaction step is the dissociation between the (−)-cocaine benzoyl group and S198 of the enzyme. The QM/MM-optimized geometries of the reactant, intermediates, and transition states are shown in Figures 1–4. The values of 10 key internuclear distances reflecting the geometrical changes are also given in Tables 1 and 2 for the acylation and deacylation stages, respectively. Below, we discuss each of these reaction steps in detail.

Step 1: Nucleophilic Attack on the C^ζ Atom by the O^γ Atom of S198. The nucleophilic attack process proceeds as the serine hydroxyl oxygen, i.e., the O^γ atom of S198, gradually approaches the C^ζ atom of (−)-cocaine benzoyl ester. Meanwhile, the serine hydroxyl hydrogen, i.e., the H^γ atom of S198, gradually moves toward the nitrogen (N^e) atom of the H438 side chain. Since this reaction step involves the breaking of the $O^\gamma-H^\gamma$ bond and the formation of both $C^\zeta-O^\gamma$ and N^e-H^γ bonds, as shown in Scheme 1, the distance between O^γ and H^γ ($R_{O^\gamma-H^\gamma}$), the distance between C^ζ and O^γ ($R_{C^\zeta-O^\gamma}$), and the distance between N^e and H^γ ($R_{N^e-H^\gamma}$) reflect the nature of chemical reaction step 1. Therefore, the reaction coordinate for the current reaction step was set as $R_{O^\gamma-H^\gamma} - R_{C^\zeta-O^\gamma} - R_{N^e-H^\gamma}$. As shown in the QM/MM-optimized geometries (Figure 1), while the O^γ atom of S198 gradually approaches the C^ζ atom, the geometry of the reactant (ES), in which the C^ζ atom is sp^2 hybridized and is in a planar geometry with its three bonding

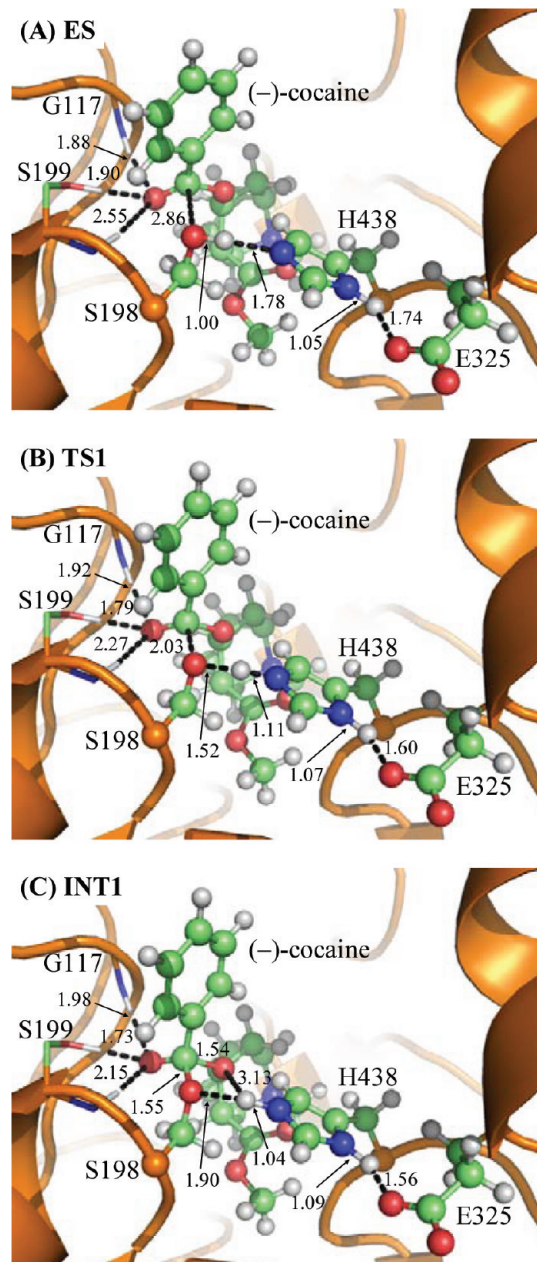


Figure 1. Key states for the reaction step 1, the nucleophilic attack by the O^γ atom of the S198 side chain. The geometries were optimized at the QM/MM(B3LYP/6-31G*:AMBER) level. The nonpolar hydrogen atoms in the oxyanion hole are not shown for clarity. The key distances in the figure are in angstroms. Carbon, oxygen, nitrogen, and hydrogen atoms are colored in green, red, blue, and white, respectively. The backbone of the protein is rendered as a cartoon and colored in orange. The QM atoms are represented as balls and sticks, and the surrounding residues are rendered as sticks. The figures below are represented using the same method.

atoms, gradually changes into a tetrahedral geometry centering on the sp^3 hybridized C^ζ atom in an intermediate (INT1) through a transition state (TS1).

Step 2: Dissociation of (−)-Cocaine Benzoyl Ester. In this reaction step, the ecgonine group of (−)-cocaine gradually departs from the (−)-cocaine benzoyl ester group in which the benzoyl ester bond $C^\zeta-O^\zeta$ is broken. Meanwhile, the proton (H^ζ) attached to N^e atom of the H438 side chain transfers to the benzoyl ester oxygen (O^ζ) of (−)-cocaine. The changes of

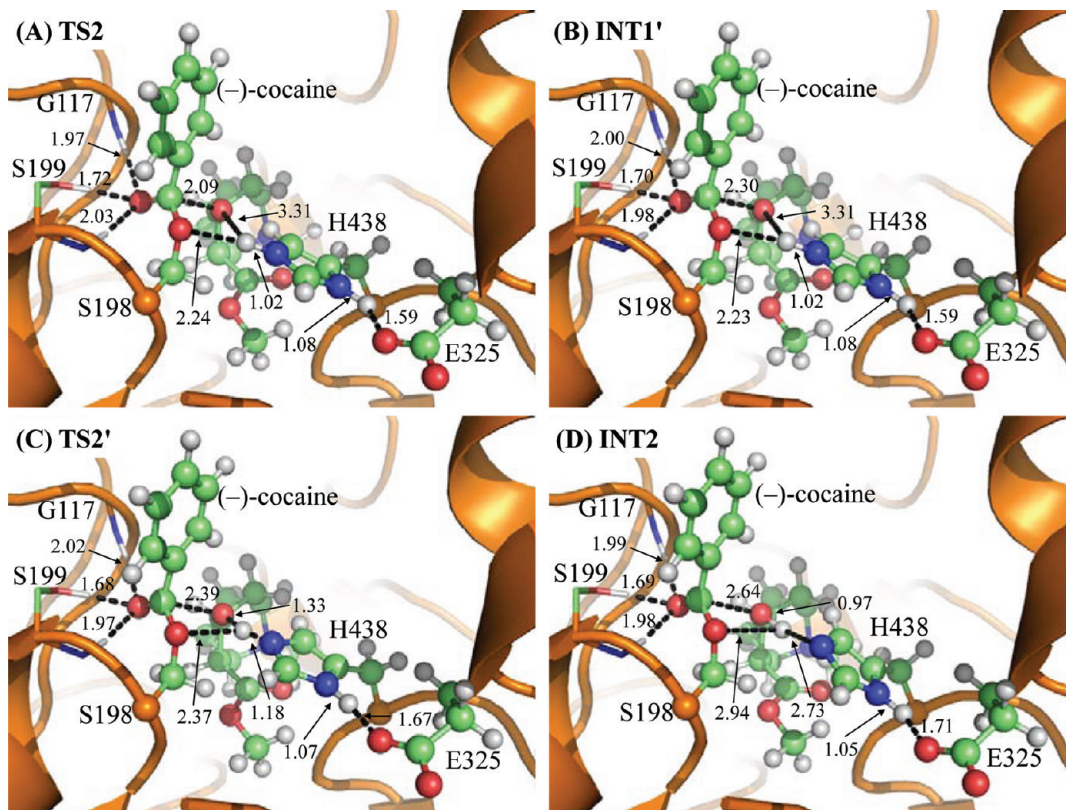


Figure 2. Key states except INT1 for reaction step 2, the dissociation of $(-)$ -cocaine benzoyl ester. The geometries were optimized at the QM/MM(B3LYP/6-31G*:AMBER) level. The structure of INT1 is given in Figure 1C.

the distances of $R_{C\zeta-O\zeta}$, $R_{O\zeta-H\gamma}$, and $R_{N\epsilon-H\gamma}$ reflect the nature of the dissociation process. Thus, the reaction coordinate for reaction step 2 was chosen as $R_{C\zeta-O\zeta} + R_{N\epsilon-H\gamma} - R_{O\zeta-H\gamma}$.

Contrary to what we proposed in Scheme 1, where only one transition state is hypothesized for reaction step 2, two transition states were found in the current reaction step. This observation is similar to that in CocE-catalyzed $(-)$ -cocaine hydrolysis where two transition states were characterized in the dissociation of $(-)$ -cocaine benzoyl ester.⁵¹ The two transition states here are denoted by TS2 and TS2', respectively. The intermediate between the two transition states is labeled as INT1'. The QM/MM-optimized geometries of the intermediates and transition states of the current reaction step are given in Figure 2. In the geometry of INT1 (Figure 1C), where the serine hydroxyl proton (H^{γ}) has been transferred to the N^{ϵ} atom of H438 in reaction step 1, the distance ($R_{O\gamma-H\gamma}$) between the O^{γ} atom of S198 and the H^{γ} atom of the H438 side chain is 1.90 Å, indicating a strong hydrogen bond of $N^{\epsilon}-H^{\gamma}\cdots O^{\gamma}$ between the S198 hydroxyl oxygen and H438 side chain. However, the distance ($R_{O\zeta-H\gamma}$) between H^{γ} and the leaving ester oxygen (O^{ζ}) to which H^{γ} is about to be transferred is 3.13 Å, indicating a very weak interaction between the H^{γ} and O^{ζ} atoms and an unfavorable environment for proton transfer from the N^{ϵ} atom of H438 to the leaving ester oxygen (O^{ζ}) atom. In the substep of changing from INT1 to INT1', the major structural change is the gradual breaking of the covalent bond $C^{\zeta}-O^{\zeta}$ ($R_{C\zeta-O\zeta}$ is 1.54 Å in INT1, 2.09 Å in TS2, and 2.30 Å in INT1'). During this process, $R_{O\zeta-H\gamma}$ does not decrease but slightly increases from 3.13 Å in INT1 to 3.31 Å in TS2 and remains this distance until reaching INT1'. The changes of $R_{O\zeta-H\gamma}$ indicate that H438, one of the catalytic-triad residues, does not facilitate the breaking of covalent bond $C^{\zeta}-O^{\zeta}$ in the

substep of changing from INT1 to INT1'. However, in the substep of changing from INT1' to INT2, the H^{γ} atom is gradually transferred to the leaving ester oxygen (O^{ζ}) from the H438 side chain as the covalent bond $C^{\zeta}-O^{\zeta}$ is continuously breaking ($R_{C\zeta-O\zeta}$ is 2.30 Å in INT1', 2.39 Å in TS2', and 2.64 Å in INT2), suggesting that H438 begins to facilitate the breaking of covalent bond $C^{\zeta}-O^{\zeta}$ in the substep of changing from INT1' to INT2. Clearly, the proton transfer in reaction step 2 proceeds not simultaneously with but almost after the breaking of the $C^{\zeta}-O^{\zeta}$ covalent bond, and H438 facilitates this covalent bond breaking only in the substep associated with TS2'.

Step 3: Nucleophilic Attack on the C^{ζ} Atom by a Water Molecule. The ecgonine methyl ester was removed from the above-discussed QM/MM-optimized geometry of INT2 to construct the initial structure of INT2' for the reaction coordinate calculations on the deacylation stage. The current nucleophilic process proceeds in a similar way to that in reaction step 1, which involves the breaking of the $O^{\omega}-H^{\omega}$ bond and the formation of both $C^{\zeta}-O^{\omega}$ and $N^{\epsilon}-H^{\omega}$ bonds. Thus, the distances $R_{O\omega-H\omega}$, $R_{C\zeta-O\omega}$, and $R_{N\epsilon-H\omega}$ were chosen to establish the reaction coordinate as $R_{O\omega-H\omega} - R_{C\zeta-O\omega} - R_{N\epsilon-H\omega}$ for the current reaction step. In proceeding from INT2' to INT3 through the transition state TS3 (Figure 3), the nucleophilic water gradually approaches the C^{ζ} atom with a spontaneous proton (H^{ω}) transfer from the O^{ω} atom of the nucleophilic water to the N^{ϵ} atom of the H438 side chain. The QM/MM-optimized geometry of INT3 shows that the nucleophilic attack process is completed with a water molecule dissociating into a hydroxide ion attaching to the C^{ζ} atom and a proton (H^{ω}) attaching to the N^{ϵ} atom.

Step 4: Dissociation between the $(-)$ -Cocaine Benzoyl Group and S198. The proton transfer between the N^{ϵ} atom of

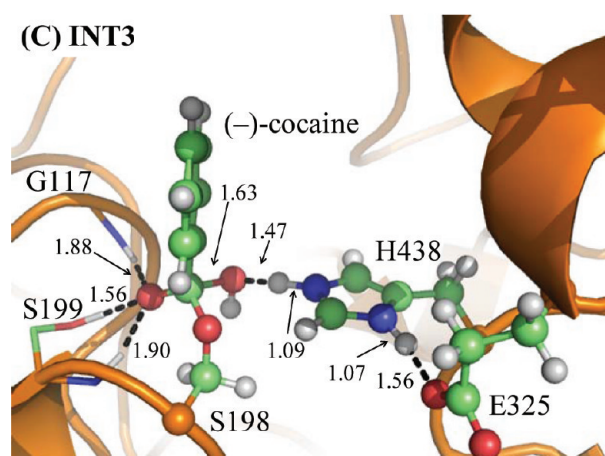
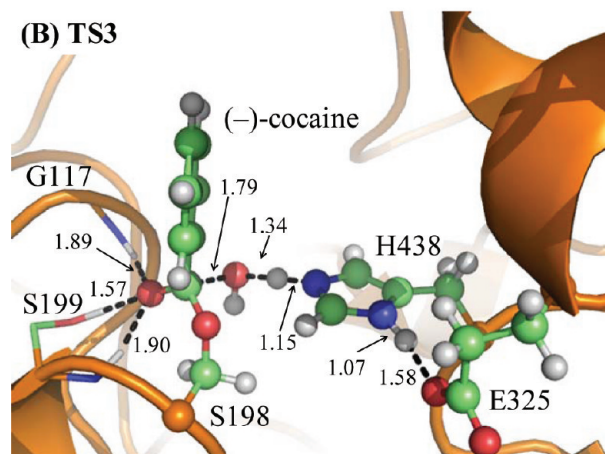
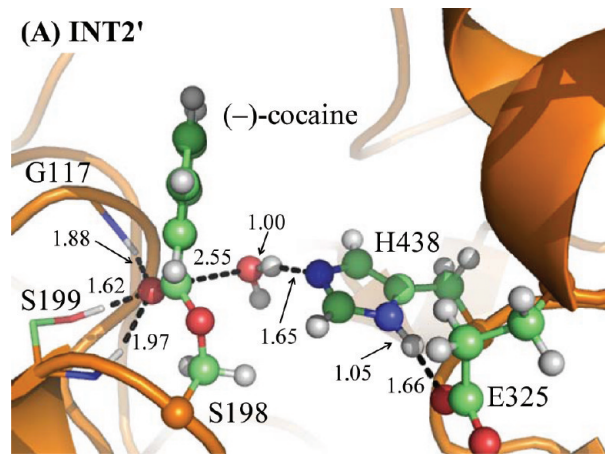


Figure 3. Key states for reaction step 3, the nucleophilic attack on the benzoyl carbonyl carbon atom by a water molecule. The geometries were optimized at the QM/MM(B3LYP/6-31G*:AMBER) level.

the H438 side chain and the O^γ atom of the S198 side chain and the breaking of covalent bond C^ζ–O^γ are involved in the dissociation of the benzoyl enzyme. The changes of the distances $R_{C^{\zeta}-O^{\gamma}}$, $R_{O^{\gamma}-H^{\omega}}$, and $R_{N^e-H^{\omega}}$ reflect the nature of reaction step 4. Thus, the reaction coordinate for the current reaction step was expressed as $R_{C^{\zeta}-O^{\gamma}} + R_{N^e-H^{\omega}} - R_{O^{\gamma}-H^{\omega}}$. Reaction step 4 is similar to reaction step 2, the dissociation of benzoyl ester. In both reaction steps, one type of C–O covalent bond is broken and one proton is transferred from the N^e atom of H438 to the oxygen atom of the broken C–O covalent

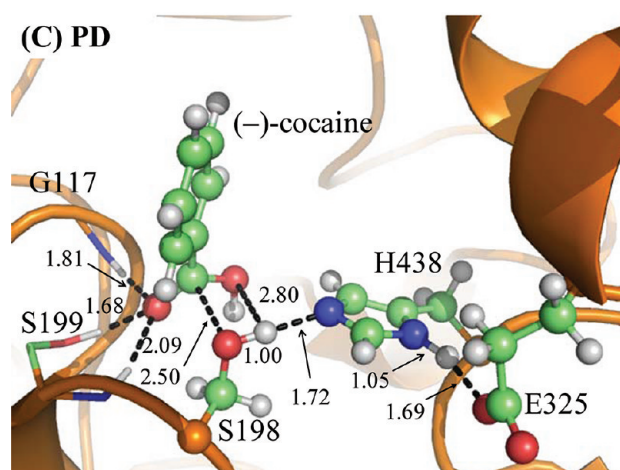
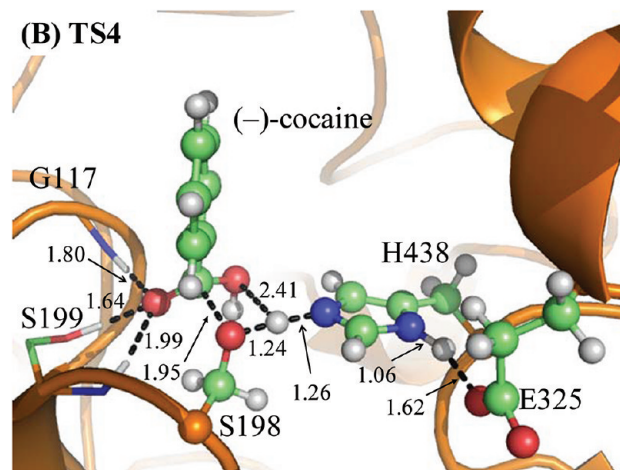
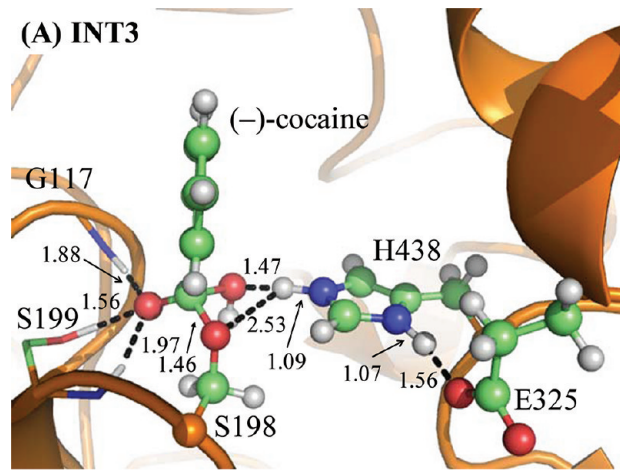


Figure 4. Key states for step 4, the dissociation of the (-)-cocaine benzoyl group from S198 of the enzyme. The geometries were optimized at the QM/MM(B3LYP/6-31G*:AMBER) level.

bond. There are differences between reaction steps 2 and 4. One difference is that the proton transfer in the current reaction step proceeds spontaneously as the C–O bond is gradually broken, while that in reaction step 2 does not proceed spontaneously. As shown in Figure 4, while the C^ζ–O^γ covalent bond gradually breaks, the distance between the O^γ atom and the H^ω atom becomes closer and closer, illustrating a spontaneous proton transfer from the N^e atom of the H438 side chain to the O^γ atom of S198. The other difference is that,

Table 1. Key Internuclear Distances (D1–D10, in Ångstrom) in the QM/MM-Optimized Geometries of the Key States of the Acylation Stage

	ES	TS1	INT1	TS2	INT1'	TS2'	INT2
D1	1.88	1.92	1.98	1.97	2.00	2.02	1.99
D2	1.90	1.79	1.73	1.72	1.70	1.68	1.69
D3	2.55	2.27	2.15	2.03	1.98	1.97	1.98
D4	2.86	2.03	1.55	1.39	1.37	1.35	1.33
D5	1.00	1.52	1.90	2.24	2.23	2.37	2.94
D6	1.78	1.11	1.04	1.02	1.02	1.18	2.73
D7	3.69	3.09	3.13	3.31	3.31	1.33	0.97
D8	1.36	1.42	1.54	2.09	2.30	2.39	2.64
D9	1.05	1.07	1.09	1.08	1.08	1.07	1.05
D10	1.74	1.60	1.56	1.59	1.59	1.67	1.71

Table 2. Key Internuclear Distances (D1–D10, in Ångstrom) in the QM/MM-Optimized Geometries of the Key States of the Deacylation Stage

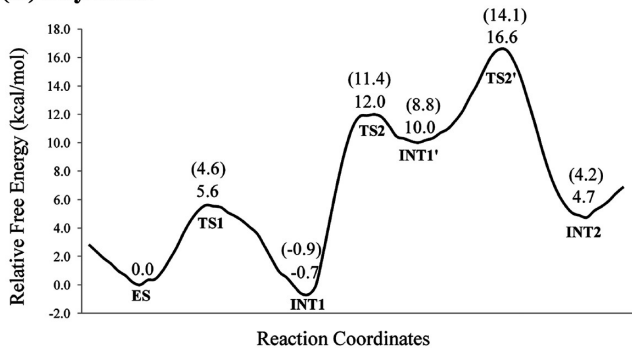
	INT2'	TS3	INT3	TS4	PD
D1	1.88	1.89	1.88	1.80	1.81
D2	1.62	1.57	1.56	1.64	1.68
D3	1.97	1.90	1.90	1.99	2.09
D4	2.55	1.79	1.63	1.40	1.35
D5	1.00	1.34	1.47	2.41	2.80
D6	1.65	1.15	1.09	1.26	1.72
D7	2.77	2.58	2.53	1.24	1.00
D8	1.34	1.42	1.46	1.95	2.50
D9	1.05	1.07	1.07	1.06	1.05
D10	1.66	1.58	1.56	1.62	1.69

since the proton is spontaneously transferred while the $C^{\prime\prime}-O^{\prime\prime}$ covalent bond gradually breaks, the H438 facilitates the breaking of the $C^{\prime\prime}-O^{\prime\prime}$ covalent bond throughout the current reaction step, whereas in reaction step 2 the H438 facilitates the breaking of the $C^{\prime\prime}-O^{\prime\prime}$ covalent bond only in the substep associated with TS2'.

Energetics. Using the QM/MM-optimized geometries at the QM/MM(B3LYP/6-31G*:AMBER) level, we carried out QM/MM single-point energy calculations at the QM/MM-(MP2/6-31+G*:AMBER) level for each geometry along the minimum-energy path for both acylation and deacylation

stages. For each geometry along the minimum-energy path, the ESP charges determined in the QM part of the QM/MM single-point energy calculation were used in subsequent FEP simulations for estimating the free energy changes along the reaction path. Depicted in Figure 5 is the energy profile determined by the QM/MM-FE calculations excluding the zero-point and thermal corrections for the QM subsystem. The values given in the parentheses are the corresponding relative free energies with the zero-point and thermal corrections for the QM subsystem. The relative free energy was taken as the average of the “forward” and “backward” perturbation results in

(A) Acylation



(B) Deacylation

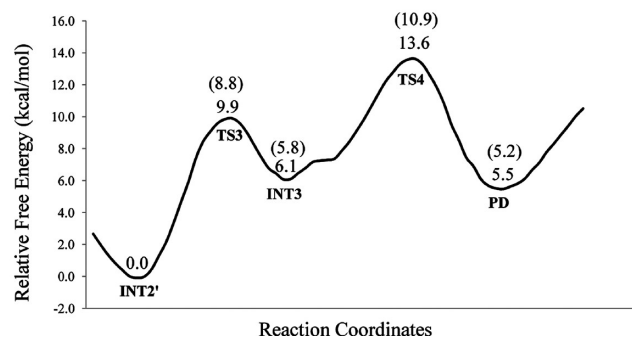


Figure 5. Free energy profile determined by performing the QM/MM-FE calculations at the MP2/6-31+G*:AMBER level excluding the zero-point and thermal corrections for the QM subsystem. The values in parentheses are relative free energies including zero-point and thermal corrections for the QM subsystem.

which the difference between the “forward” and “backward” perturbation results was 0.9 kcal/mol (suggesting an error of ± 0.5 kcal/mol) for the calculated overall free energy barrier of the acylation stage and 0.2 kcal/mol (suggesting an error of ± 0.1 kcal/mol) for the calculated overall free energy barrier of the deacylation stage. The differences between the “forward” and the “backward” perturbations are reasonably small, suggesting that the FEP calculations converged well in terms of the number of the FEP windows used.

As clearly shown in Figure 5A, there are three transition states in the acylation stage. Technically, there are a total of five reaction steps for the entire hydrolysis reaction, instead of the four reaction steps hypothesized in Scheme 1. Nevertheless, in order to clearly describe the hydrolysis mechanism, we still keep the notation used in Scheme 1. This means that reaction step 2, which is the dissociation of (−)-cocaine benzoyl ester, consists of two substeps associated with TS2 and TS2'. The free energy barriers with zero-point and thermal corrections for the QM subsystem of the two substeps associated with the TS2 and TS2' are ~ 12.3 and ~ 5.3 kcal/mol, respectively. The free energy of TS2' is higher than that of TS2. Therefore, the overall free energy barrier of the entire reaction step 2, i.e., the free energy change from the INT1 to TS2', is ~ 15.0 kcal/mol, which is higher than the corresponding energy barrier for reaction step 1 (~ 4.5 kcal/mol). As a result, reaction step 2 is rate-determining for the acylation stage. In the deacylation stage, the free energy barriers with zero-point and thermal corrections for the QM subsystem of reaction steps 3 and 4 are ~ 8.8 and ~ 5.1 kcal/mol, respectively. The free energy of TS4 is higher than that of TS3, and therefore, the free energy change (~ 10.9 kcal/mol) from INT2' to TS4 is the overall free energy

barrier for the deacylation stage. Obviously, reaction step 2 in the acylation stage, where the free energy barrier is ~ 15.0 kcal/mol, is rate-determining for the whole (−)-cocaine hydrolysis catalyzed by the A199S/F227A/S287G/A328W/Y332G mutant of human BChE. The calculated free energy barrier of ~ 15.0 kcal/mol is in excellent agreement with the activation free energy of 14.7 kcal/mol derived from the experimental rate constant ($k_{\text{cat}} = 5700 \text{ min}^{-1}$)¹³ by using the conventional transition state theory (CTST).^{12,57,58} On the basis of the mechanistic insights, future computational design aiming at further improving the catalytic activity of the cocaine hydrolase against (−)-cocaine should focus on the stabilization of the transition state (TS2') for the second reaction step.

The Role of Catalytic Triad and Oxyanion Hole.

According to the mechanism described by the pseudobond first-principles QM/MM-FE calculations, the catalytic triad and oxyanion hole are the most essential factors in the (−)-cocaine hydrolysis. The first residue in the catalytic triad, S198, acts as a nucleophile in reaction step 1 and then forms a covalent bond with the carbonyl carbon (C^ζ) atom of (−)-cocaine benzoyl ester until the end of hydrolysis reaction. The second residue in catalytic triad, H438, serves as a general base, accepting the proton from the nucleophile to facilitate the two nucleophilic attack processes, i.e., reaction steps 1 and 3. The proton is then transferred to the leaving group by H438 in the two dissociation processes, i.e., reaction steps 2 and 4. H438 facilitates either the formation or breaking of the C–O covalent bond in each reaction step. As seen from Figures 2–5, H438 is in turn stabilized by E325 via a strong hydrogen bond of $N^\delta-H^\delta\cdots O^\delta$ between their side chains throughout the entire hydrolysis process. Note that in reaction step 2, which is rate-determining, H438 does not facilitate the breaking of the $C^\zeta-O^\zeta$ covalent bond in the very beginning but starts to stabilize the negatively charged O^ζ atom only in the substep associated with TS2'. An effort aiming at releasing the facilitation function of H438 at the very beginning of the breaking of the $C^\zeta-O^\zeta$ covalent bond is thus very promising in stabilizing TS2' and decreasing the rate-determining energy barrier.

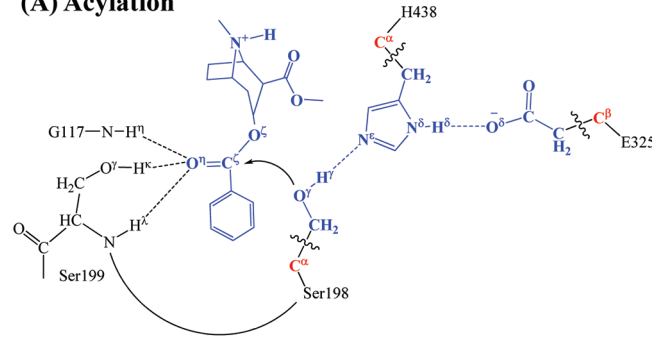
The oxyanion hole consists of the backbone amides of S199 and G117 and the hydroxyl group of S199. On the basis of the QM/MM reaction coordinate calculations, the carbonyl oxygen (O^η) of (−)-cocaine forms three hydrogen bonds with the oxyanion hole throughout the hydrolysis reaction. One is the hydrogen bond of $N-H^\eta\cdots O^\eta$ with the backbone NH group (H^η) of G117. The second is the hydrogen bond of $O^\gamma-H^\kappa\cdots O^\eta$ with the hydroxyl hydrogen (H^κ) of the S199 side chain. The third is the hydrogen bond of $N-H^\lambda\cdots O^\eta$ with the backbone NH group (H^λ) of S199. As shown in Figure 1A, there are two strong ($N-H^\eta\cdots O^\eta$ and $O^\gamma-H^\kappa\cdots O^\eta$) and one weak ($N-H^\lambda\cdots O^\eta$) hydrogen bond in the structure of ES. The $N-H^\lambda\cdots O^\eta$ is weak in ES with a $H^\lambda\cdots O^\eta$ distance of ~ 2.6 Å and then becomes strong with a $H^\lambda\cdots O^\eta$ distance of ~ 2.0 Å in the subsequent states of the hydrolysis reaction. The other two hydrogen bonds $N-H^\eta\cdots O^\eta$ and $O^\gamma-H^\kappa\cdots O^\eta$ are steadily strong throughout the hydrolysis reaction, with the $H^\eta\cdots O^\eta$ and $H^\kappa\cdots O^\eta$ distances being ~ 1.9 Å and ~ 1.6 Å, respectively. Therefore, all three of these hydrogen bonds stabilize the negative charge of the carbonyl oxygen (O^η) that develops during the hydrolysis reaction.

METHODS

Structure Preparation. The starting model of the system was based on our previously reported molecular dynamics (MD) simulation performed on the first transition state (TS1) for the A199S/F227A/S287G/A328W/Y332G mutant of BChE with (−)-cocaine.¹³ In the MD simulation, the system was solvated in a rectangular box of TIP3P water molecules with a minimum solute-wall distance of 10 Å. It was gradually heated from $T = 10$ K to $T = 298.15$ K over 30 ps before running the MD simulation at $T = 298.15$ K for ~ 2 ns. The time step used for the MD simulation was 2 fs. The SHAKE algorithm was used to fix all covalent bonds containing hydrogen atoms. The particle mesh Ewald (PME) method was used to treat long-range electrostatic interactions. In the present study, a snapshot close to the average structure from the MD simulation was used to prepare the initial structure for the QM/MM calculations. Since the ecgonine group of (−)-cocaine leaves the system after the acylation stage, the structure of INT2' was constructed by removing the ecgonine group of (−)-cocaine out of the QM/MM-optimized INT2 structure. The constructed INT2' was also solvated in a rectangular box of TIP3P water molecules with a minimum solute-wall distance of 10 Å and was then equilibrated by performing a ~ 2 ns MD simulation with the same procedure mentioned above. A snapshot close to the average structure from this MD simulation was selected to prepare the initial structure of INT2' for the QM/MM reaction-coordinate calculations. Since we are interested in the reaction center, the water molecules beyond 50 Å of the carbonyl carbon (C^ζ) of the (−)-cocaine benzoyl ester were removed in the preparation of initial reaction systems. Prior to the QM/MM geometry optimizations, the initial reaction systems were energy-minimized with the MM method by using the revised AMBER8 program,⁵¹ where the convergence criterion is the root-mean-square deviation (RMSD) of the energy gradient being smaller than 0.1 kcal mol^{−1} Å^{−1}.

QM/MM-FE Simulation. All of the QM/MM calculations were performed by using the pseudobond QM/MM method^{35,36} implemented recently in a revised version¹³ of Gaussian 03⁵⁹ and AMBER8⁶⁰ programs. The QM/MM interface was treated by the pseudobond approach, where a seven-valence-electron atom with an effective core potential is constructed to replace the boundary atom of the environment part and to form a pseudobond with the boundary atom of the active part. In QM/MM calculations, all atoms of (−)-cocaine and the side chains of S198, H438, and E325 were considered as the QM atoms, whereas the other atoms were regarded as MM atoms (Figure 6). The QM/MM calculations were performed with an iterative minimization procedure³⁷ at the B3LYP/6-31G*:AMBER level; i.e., the QM calculations were carried out at the B3LYP/6-31G* level, whereas the MM calculations were carried out by using the AMBER force field implemented in the AMBER8 program.⁶⁰ For the QM subsystem, the convergence criterion for geometry optimizations follows the original Gaussian 03⁵⁹ defaults; for the MM subsystem, the geometry optimization convergence criterion is a RMSD of the energy gradient less than 0.1 kcal mol^{−1} Å^{−1}. An iterative restrained optimization procedure³⁷ was then repeatedly applied to different points along the reaction coordinate, resulting in a minimum-energy path. Full QM/MM geometry-optimizations at the B3LYP/6-31G*:AMBER level followed by vibrational frequency analyses were performed

(A) Acylation



(B) Deacylation

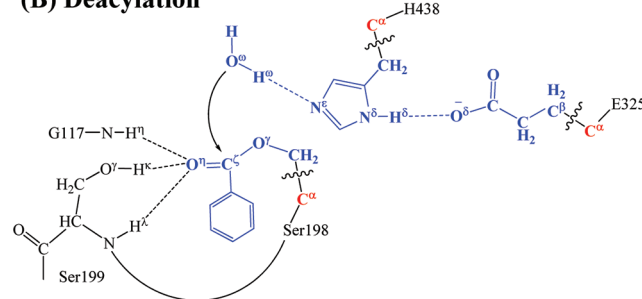


Figure 6. Division of the QM/MM systems for simulating the (−)-cocaine hydrolysis catalyzed by the A199S/F227A/S287G/A328W/Y332G mutant of BChE. Atoms in blue are treated by the QM method. Three boundary carbon atoms (C^α or C^β , colored in red) are treated with the improved pseudobond parameters.³⁵ All other atoms belong to the MM subsystem.

to characterize the reactant, intermediates, and transition states. The contribution of the QM subsystem fluctuation to the free energy change was then calculated with obtained frequencies using the harmonic approximation. In addition, single-point energy calculations were carried out at the QM/MM(MP2/6-31+G*:AMBER) level for each geometry along the minimum-energy path.

The free energy changes associated with the QM-MM interaction were then determined by the free energy perturbation (FEP) method^{37,61} using a revised version⁵¹ of the AMBER8 program. The FEP calculations enabled us to more reasonably determine the relative free energy changes due to the QM-MM interaction. In FEP calculations, sampling of the MM subsystem was carried out with the QM subsystem frozen at different states along the reaction path.³⁷ Technically, the final (relative) free energy determined by the QM/MM-FE calculations is the QM part of the QM/MM energy (excluding the Columbic interaction energy between the point charges of the MM atoms and the ESP charges of the QM atoms) plus the relative free energy change determined by the FEP calculations. In FEP calculations, the time step used was 2 fs, and bond lengths involving hydrogen atoms were constrained. In sampling of the MM subsystem using MD simulations, the temperature was maintained at 298.15 K. Each window of the FEP calculation consisted of 50 ps of equilibration and 300 ps of sampling. The choice of the 300 ps sampling for each window was based on the observation that there was no noticeable difference between the FEP results obtained from the 300 ps sampling and those from the 500 ps sampling for the rate-determining step of the enzymatic reaction process. Both the forward and backward reaction directions were subjected to

the FEP calculations. The final relative free energies were taken as the average of the “forward” and “backward” perturbation results.

The MD simulations and QM/MM-FE calculations were performed on a supercomputer (e.g., IBM X-series Cluster with 340 nodes or 1360 processors) at the University of Kentucky Center for Computational Sciences. The other, less time-consuming modeling and computations were carried out on SGI Fuel workstations and a 34-processor IBM x335 Linux cluster in our own lab.

CONCLUSION

The (−)-cocaine hydrolysis catalyzed by the cocaine hydrolase (i.e., the A199S/F227A/S287G/A328W/Y332G mutant of human BChE) has been studied by using a first-principles QM/MM-FE approach. The detailed reaction pathway has been elucidated. First, a nucleophilic attack on the carbonyl carbon (C^ζ) of (−)-cocaine benzoyl ester is carried out by the hydroxyl oxygen (O^γ) of S198. This process is facilitated by H438 through proton (H^γ) transfer from the S198 hydroxyl to the N^c atom of the H438 side chain, which increases the nucleophilicity of the S198 hydroxyl. H438 is in turn stabilized by another hydrogen bond with E325. The S198 nucleophile attacks the electron-deficient C^ζ atom, forming a tetrahedral intermediate, in which the carbonyl oxygen (O^η) of (−)-cocaine with developing negative charge is stabilized through three hydrogen bonds formed with the oxyanion hole. Then, H438 transfers the proton (H^γ) to the ester oxygen (O^ζ) of the leaving ecgonine group, completing the acylation stage. Starting from the acylated enzyme, a water molecule which is activated by H438 initiates the deacylation stage. Reaction steps similar to those in the acylation stage are repeated in the deacylation stage in terms of the covalent bond formation and breaking, and the benzoic acid is released while the original enzyme form is restored to its free state. The second reaction step of the entire reaction process, where the benzoyl ester dissociates, is found to be rate-determining. The calculated free energy barrier is ~15.0 kcal/mol and is in excellent agreement with the experimentally derived activation free energy of ~14.7 kcal/mol.

The QM/MM-optimized geometries indicate that oxyanion hole stabilizes the negative charge of the carbonyl oxygen developing during the hydrolysis reaction by providing three hydrogen bonds from backbone amides of S199 and G117 and the hydroxyl group of S199. The hydrogen bond with hydroxyl group of S199 is further confirmed to have an important contribution to stabilizing the transition state for the rate-determining step.

The elucidated reaction mechanism provides details of the hydrolysis reaction, especially the rate-determining step and the nature of the transition states. In light of new mechanistic insights obtained in the present investigation, future efforts aiming at further increasing the catalytic activity of the cocaine hydrolase against (−)-cocaine should focus on reaction step 2, i.e., the dissociation of the benzoyl ester. Note that H438 does not facilitate the breaking of the $C^\zeta-O^\zeta$ covalent bond in the very beginning of reaction step 2. An effort of releasing the facilitation function of H438 on the breaking of the $C^\zeta-O^\zeta$ covalent bond immediately when the $C^\zeta-O^\zeta$ covalent bond starts to break is thus very likely to further improve the catalytic activity of the cocaine hydrolase against (−)-cocaine. Thus, the new mechanistic insights obtained from the present computational study will be of value for the future rational design of

more efficient cocaine hydrolase to be used in the treatment of cocaine overdose and abuse.

AUTHOR INFORMATION

Corresponding Author

*Phone: 859-323-3943. Fax: 859-323-3575. E-mail: zhan@uky.edu.

Notes

The authors declare no competing financial interest.

ACKNOWLEDGMENTS

This work was supported in part by NIH (grants R01 DA013930 and R01 DA025100). J.L. worked in C.-G.Z.’s laboratory for this project as a visiting scientist under NIH funding support. The entirety of the research was performed at the University of Kentucky. The authors acknowledge the Center for Computational Sciences (CCS) at the University of Kentucky for supercomputing time on the IBM X-series Cluster with 340 nodes or 1360 processors.

REFERENCES

- (1) Mendelson, J. H.; Mello, N. K. *N. Engl. J. Med.* **1996**, *334*, 965–972.
- (2) Paula, S.; Tabet, M. R.; Farr, C. D.; Norman, A. B.; Ball, W. J. *J. Med. Chem.* **2003**, *47*, 133–142.
- (3) Singh, S. *Chem. Rev.* **2000**, *100*, 925–1024.
- (4) Huang, X.; Zheng, F.; Zhan, C.-G. *J. Phys. Chem. B* **2011**, *115*, 11254–11260.
- (5) Meijler, M. M.; Kaufmann, G. F.; Qi, L.; Mee, J. M.; Coyle, A. R.; Moss, J. A.; Wirsching, P.; Matsushita, M.; Janda, K. D. *J. Am. Chem. Soc.* **2005**, *127*, 2477–2484.
- (6) Sparnborg, S.; Voccia, F.; Zukin, S. *Drug Alcohol. Depend.* **1997**, *48*, 149–51.
- (7) Gorelick, D. A. *Drug Alcohol. Depend.* **1997**, *48*, 159–65.
- (8) Gorelick, D. A.; Gardner, E. L.; Xi, Z. X. *Drugs* **2004**, *64*, 1547–73.
- (9) Dickerson, T. J.; Janda, K. D. Recent Advances for the Treatment of Cocaine Abuse: Central Nervous System Immunopharmacotherapy. In *Drug Addiction*; 2008; pp 217–229.
- (10) Gao, D.; Cho, H.; Yang, W.; Pan, Y.; Yang, G.; Tai, H.-H.; Zhan, C.-G. *Angew. Chem., Int. Ed.* **2006**, *45*, 653–657.
- (11) Voccia, F. J.; Acri, J.; Elkashef, A. *Am. J. Psychiatry* **2005**, *162*, 1432–1440.
- (12) Pan, Y.; Gao, D.; Yang, W.; Cho, H.; Yang, G.; Tai, H.-H.; Zhan, C.-G. *Proc. Natl. Acad. Sci. U.S.A.* **2005**, *102*, 16656–16661.
- (13) Zheng, F.; Yang, W.; Ko, M.-C.; Liu, J.; Cho, H.; Gao, D.; Tong, M.; Tai, H.-H.; Woods, J. H.; Zhan, C.-G. *J. Am. Chem. Soc.* **2008**, *130*, 12148–12155.
- (14) Landry, D. W.; Zhao, K.; Yang, G. X.; Glickman, M.; Georgiadis, T. M. *Science* **1993**, *259*, 1899–1901.
- (15) Mets, B.; Winger, G.; Cabrera, C.; Seo, S.; Jamdar, S.; Yang, G.; Zhao, K.; Briscoe, R. J.; Almonte, R.; Woods, J. H.; Landry, D. W. *Proc. Natl. Acad. Sci. U.S.A.* **1998**, *95*, 10176–10181.
- (16) Zhan, C.-G.; Zheng, F.; Landry, D. W. *J. Am. Chem. Soc.* **2003**, *125*, 2462–74.
- (17) Rogers, C. J.; Mee, J. M.; Kaufmann, G. F.; Dickerson, T. J.; Janda, K. D. *J. Am. Chem. Soc.* **2005**, *127*, 10016–10017.
- (18) Pan, Y. M.; Gao, D. Q.; Yang, W. C.; Cho, H.; Zhan, C.-G. *J. Am. Chem. Soc.* **2007**, *129*, 13537–13543.
- (19) Sun, H.; Pang, Y.-P.; Lockridge, O.; Brimijoin, S. *Mol. Pharmacol.* **2002**, *62*, 220–224.
- (20) Zhan, C.-G.; Gao, D. Q. *Biophys. J.* **2005**, *89*, 3863–3872.
- (21) Huang, X.; Pan, Y.; Zheng, F.; Zhan, C.-G. *J. Phys. Chem. B* **2010**, *114*, 13545–13554.
- (22) Hamza, A.; Cho, H.; Tai, H.-H.; Zhan, C.-G. *J. Phys. Chem. B* **2005**, *109*, 4776–4782.

- (23) Sun, H.; El Yazal, J.; Lockridge, O.; Schopfer, L. M.; Brimijoin, S.; Pang, Y. *P. J. Biol. Chem.* **2001**, *276*, 9330–9336.
- (24) Huang, X.; Gao, D.; Zhan, C.-G. *Org. Biomol. Chem.* **2011**, *9*, 4138–4143.
- (25) Yang, W.; Pan, Y.; Zheng, F.; Cho, H.; Tai, H.-H.; Zhan, C.-G. *Biophys. J.* **2009**, *96*, 1931–1938.
- (26) Yang, W. C.; Xue, L.; Fang, L.; Chen, X.; Zhan, C.-G. *Chem. Biol. Interact.* **2010**, *187*, 148–152.
- (27) Zheng, F.; Yang, W. C.; Xue, L.; Hou, S. R.; Liu, J. J.; Zhan, C.-G. *Biochemistry* **2010**, *49*, 9113–9119.
- (28) Gao, Y.; Orson, F. M.; Kinsey, B.; Kosten, T.; Brimijoin, S. *Chem. Biol. Interact.* **2010**, *187*, 421–424.
- (29) Adrian, J. M. *Drug Discovery Today* **2005**, *10*, 1393–1402.
- (30) Cavalli, A.; Carloni, P.; Recanatini, M. *Chem. Rev.* **2006**, *106*, 3497–3519.
- (31) Menikarachchi, L. C.; Gascon, J. A. *Curr. Top. Med. Chem.* **2010**, *10*, 46–54.
- (32) Raha, K.; Peters, M. B.; Wang, B.; Yu, N.; WollaCott, A. M.; Westerhoff, L. M.; Merz, K. M. *Drug Discovery Today* **2007**, *12*, 725–731.
- (33) Zhou, T.; Huang, D. Z.; Caflisch, A. *Curr. Top. Med. Chem.* **2010**, *10*, 33–45.
- (34) De Vivo, M. *Front. Biosci.* **2011**, *16*, 1619–1633.
- (35) Zhang, Y. K. *J. Chem. Phys.* **2005**, *122*, 024114.
- (36) Zhang, Y. K.; Lee, T. S.; Yang, W. T. *J. Chem. Phys.* **1999**, *110*, 46–54.
- (37) Zhang, Y. K.; Liu, H. Y.; Yang, W. T. *J. Chem. Phys.* **2000**, *112*, 3483–3492.
- (38) Zhang, Y. K. *Theor. Chem. Acc.* **2006**, *116*, 43–50.
- (39) Hu, P.; Zhang, Y. K. *J. Am. Chem. Soc.* **2006**, *128*, 1272–1278.
- (40) Liu, H.; Zhang, Y.; Yang, W. *J. Am. Chem. Soc.* **2000**, *122*, 6560–6570.
- (41) Zhang, Y.; Kua, J.; McCammon, J. A. *J. Am. Chem. Soc.* **2002**, *124*, 10572–10577.
- (42) Cisneros, G. A.; Liu, H.; Zhang, Y.; Yang, W. *J. Am. Chem. Soc.* **2003**, *125*, 10384–10393.
- (43) Zhang, Y.; Kua, J.; McCammon, J. A. *J. Phys. Chem. B* **2003**, *107*, 4459–4463.
- (44) Cheng, Y.; Zhang, Y.; McCammon, J. A. *J. Am. Chem. Soc.* **2005**, *127*, 1553–1562.
- (45) Corminboeuf, C.; Hu, P.; Tuckerman, M. E.; Zhang, Y. *J. Am. Chem. Soc.* **2006**, *128*, 4530–4531.
- (46) Wang, L.; Yu, X.; Hu, P.; Broyde, S.; Zhang, Y. *J. Am. Chem. Soc.* **2007**, *129*, 4731–4737.
- (47) Wang, S.; Hu, P.; Zhang, Y. *J. Phys. Chem. B* **2007**, *111*, 3758–3764.
- (48) Xiao, C.; Zhang, Y. *J. Phys. Chem. B* **2007**, *111*, 6229–6235.
- (49) Hu, P.; Wang, S.; Zhang, Y. *J. Am. Chem. Soc.* **2008**, *130*, 3806–3813.
- (50) Cheng, Y.; Zhang, Y.; McCammon, J. A. *Protein Sci.* **2006**, *15*, 672–683.
- (51) Liu, J.; Hamza, A.; Zhan, C.-G. *J. Am. Chem. Soc.* **2009**, *131*, 11964–75.
- (52) Gao, D. Q.; Zhan, C.-G. *J. Phys. Chem. B* **2005**, *109*, 23070–23076.
- (53) Zheng, F.; Zhan, C.-G. *Org. Biomol. Chem.* **2008**, *6*, 836–843.
- (54) Gao, D. Q.; Zhan, C.-G. *Proteins* **2006**, *62*, 99–110.
- (55) Zheng, F.; Zhan, C.-G. *J. Comput.-Aided Mol. Des.* **2008**, *22*, 661–671.
- (56) Zhan, C.-G. *Expert Rev. Clin. Pharmacol.* **2009**, *2*, 1–4.
- (57) Truhlar, D. G.; Garrett, B. C. *Annu. Rev. Phys. Chem.* **1984**, *35*, 159–189.
- (58) Alvarez-Idaboy, J. R.; Galano, A.; Bravo-Perez, G.; Ruiz, M. E. *J. Am. Chem. Soc.* **2001**, *123*, 8387–8395.
- (59) Frisch, M. J.; Trucks, G. W.; Schlegel, H. B.; Scuseria, G. E.; Robb, M. A.; Cheeseman, J. R.; Montgomery, J. A., Jr.; Vreven, T.; Kudin, K. N.; Burant, J. C.; Millam, J. M.; Iyengar, S. S.; Tomasi, J.; Barone, V.; Mennucci, B.; Cossi, M.; Scalmani, G.; Rega, N.; Petersson, G. A.; Nakatsuji, H.; Hada, M.; Ehara, M.; Toyota, K.; Fukuda, R.; Hasegawa, J.; Ishida, M.; Nakajima, T.; Honda, Y.; Kitao, O.; Nakai, H.; Klene, M.; Li, X.; Knox, J. E.; Hratchian, H. P.; Cross, J. B.; Bakken, V.; Adamo, C.; Jaramillo, J.; Gomperts, R.; Stratmann, R. E.; Yazayev, O.; Austin, A. J.; Cammi, R.; Pomelli, C.; Ochterski, J. W.; Ayala, P. Y.; Morokuma, K.; Voth, G. A.; Salvador, P.; Dannenberg, J. J.; Zakrzewski, V. G.; Dapprich, S.; Daniels, A. D.; Strain, M. C.; Farkas, O.; Malick, D. K.; Rabuck, A. D.; Raghavachari, K.; Foresman, J. B.; Ortiz, J. V.; Cui, Q.; Baboul, A. G.; Clifford, S.; Cioslowski, J.; Stefanov, B. B.; Liu, G.; Liashenko, A.; Piskorz, P.; Komaromi, I.; Martin, R. L.; Fox, D. J.; Keith, T.; Al-Laham, M. A.; Peng, C. Y.; Nanayakkara, A.; Challacombe, M.; Gill, P. M. W.; Johnson, B.; Chen, W.; Wong, M. W.; Gonzalez, C.; Pople, J. A. *Gaussian 03*, revision C.02; Gaussian, Inc.: Wallingford, CT, 2004.
- (60) Case, D. A.; Darden, T. A.; Cheatham, I.; Simmerling, C. L.; Wang, J.; Duke, R. E.; Luo, R.; Merz, K. M.; Wang, B.; Pearlman, D. A.; Crowley, M.; Brozell, S.; Tsui, V.; Gohlke, H.; Mongan, J.; Hornak, V.; Cui, G.; Beroza, P.; Schafmeister, C.; Caldwell, J. W.; Ross, W. S.; Kollman, P. A. *AMBER 8*; University of California: San Francisco, CA, 2004.
- (61) Zhang, Y.; Liu, H.; Yang, W. Ab initio qm/mm and free energy calculations of enzyme reactions. In *Computational Methods for Macromolecular Modeling-Challenges and Applications*; Schlick, T., Gan, H. H., Eds.; Springer-Verlag: New York, 2002; pp 332–354.